On the performance evaluation of LQAM-MPPM techniques over exponentiated Weibull fading free-space optical channels

Haitham S. Khallaf [a,e,*], Abdulaziz E. Elfiqi [b,e], Hossam M.H. Shalaby [c], Seiichi Sampei [d], Salah S.A. Obayya [e]

[a] *Nuclear Research Center, Egyptian Atomic Energy Authority (EAEA), Inshas 13759, Egypt*
[b] *Faculty of Electronic Engineering (FEE), Menoufia University, Menouf 32952, Egypt*
[c] *Faculty of Engineering, Alexandria University, Alexandria 21544, Egypt*
[d] *Graduate School of Engineering, Osaka University, 2-1 Yamada-oka, Suita, Osaka 565-0871, Japan*
[e] *Center for Photonics and Smart Materials (CPSM), Zewail City of Science and Technology, Giza 12588, Egypt*

A B S T R A C T

We investigate the performance of hybrid L-ary quadrature-amplitude modulation-multi-pulse pulse-position modulation (LQAM-MPPM) techniques over exponentiated Weibull (EW) fading free-space optical (FSO) channel, considering both weather and pointing-error effects. Upper bound and approximate-tight upper bound expressions for the bit-error rate (BER) of LQAM-MPPM techniques over EW FSO channels are obtained, taking into account the effects of fog, beam divergence, and pointing-error. Setup block diagram for both the transmitter and receiver of the LQAM-MPPM/FSO system are introduced and illustrated. The BER expressions are evaluated numerically and the results reveal that LQAM-MPPM technique outperforms ordinary LQAM and MPPM schemes under different fading levels and weather conditions. Furthermore, the effect of modulation-index is investigated and it turned out that a modulation-index greater than 0.4 is required in order to optimize the system performance. Finally, the effect of pointing-error introduces a great power penalty on the LQAM-MPPM system performance. Specifically, at a BER of 10^{-9}, pointing-error introduces power penalties of about 45 and 28 dB for receiver aperture sizes of $D_R = 50$ and 200 mm, respectively.

1. Introduction

The importance of free-space optical (FSO) communications has increased recently because it is a very promising way of providing high speed, large capacity, and cost effective wireless data transmission [1]. However, the performance of FSO communications systems is highly affected by atmospheric conditions. One of the main phenomena that affects the performance of FSO systems is the atmospheric turbulence or scintillation, which results from inhomogeneities in the temperature and pressure of the atmosphere [2]. It leads to random fluctuations in both amplitude and phase of the received optical signal, due to variations in the refractive index, which degrade the system performance. In addition, fog and pointing-error have high degradation effect on the received optical beams [3,4].

Several statistical distributions have been assumed to characterize the atmospheric turbulence in literature. The widely accepted distributions are log-normal (LN), gamma–gamma (GG), and exponentiated Weibull (EW) models. Experimental studies support the fact that LN model is valid in weak turbulence regime for a point receiver and works well in all regimes of turbulence for aperture averaged data [5,6]. GG model is accepted to be valid in all turbulence regimes for a point receiver, nevertheless, this does not hold when aperture averaging takes place [7,5,8]. On the other hand, EW distribution offers an excellent matching with the simulation and experimental data under all aperture averaging conditions and different turbulent conditions [9]. Therefore, in this paper, we use EW distribution to characterize different channel effects on FSO transmission systems. An even more realistic scenario is considered in this paper, where the effects of fog, beam divergence, and pointing-error are taken into consideration.

In recent years, superimposing different modulation techniques to improve both power and spectral efficiencies simultaneously have been proposed [10–20]. Liu et al. have introduced a new modulation formats based on combining M-ary pulse-position modulation (m-PPM) or M-ary frequency-shift keying (m-FSK) with additional polarization

---

and/or phase modulation [10]. Hybrid modulation techniques, based on polarization-switched quadrature phase-shift keying (PS-QPSK) and polarization-division multiplexing quadrature phase-shift keying (PDM-QPSK) superimposed on pulse-position modulation (PPM) have been proposed in [11–13]. Hybrid modulation techniques, based on combining multiple-pulse pulse-position modulation (MPPM) with binary phase-shift keying (BPSK) and quadrature-phase shift keying (QPSK), have been introduced in [14,15]. A hybrid modulation technique, based on both orthogonal frequency-division multiplexing and pulse-position modulation OFDM-PPM, has been proposed in [16]. In [17], quadrature-amplitude modulation on top of multiple-pulse pulse-position modulation (QAM-MPPM) has been introduced. A hybrid differential phase-shift keying-multi-pulse pulse position modulation (DPSK-MPPM) technique is proposed and investigated in [18]. In [19,20], the maximum achievable power efficiencies of LQAM-MPPM techniques under spectral efficiency constraints are investigated and it is revealed that LQAM-MPPM is the most power efficient scheme.

In [2], we have investigated the performance of FSO systems adopting MPPM under gamma–gamma fading channel. In [21,22], analytical mathematical expressions have been derived for BER and outage probability of both QAM and PSK-OFDM radio-on-FSO system, considering fading effect, which has been modeled by a gamma–gamma distribution. In [23], Wang et al. have derived approximate expressions for symbol-error rate (SER) of MPPM under EW distribution. However, the pointing-error have not been considered in their paper. In addition, they have neglected the effects of both fog and beam divergence. In [17,24], we have investigated the performance of a hybrid QAM-MPPM system under both turbulence-free and turbulent gamma–gamma channels. We extend this work here by considering EW distribution to study the effect of aperture averaging on system performance, which is not available with GG distributions. In addition, effects of fog, beam divergence, and pointing-error are considered, which represents a more realistic scenario compared with that in [17,24].

In this paper, we aim at deriving upper bound and approximate upper bound expressions for the average BER of hybrid LQAM-MPPM over EW fading FSO transmission channel, taking into account the effects of fog, beam divergence, and pointing-error. In order to formulate these expressions, Upper bound and approximate upper bound formulas are derived for both ordinary MPPM and QAM schemes. The obtained expressions for average BER of hybrid LQAM-MPPM scheme are used to investigate and compare its performance with that of ordinary modulation schemes for different aperture sizes, fading levels, and weather conditions. In addition, the analysis and investigation are extended to include the pointing-error effect on our LQAM-MPPM/FSO transmission system. Furthermore, the effect of both modulation-index on our system is investigated. Moreover, an illustration for the setup block diagram of LQAM-MPPM/FSO system is proposed and explored.

The rest of the paper is organized as follows. In Section 2, a setup block diagram of LQAM-MPPM/FSO transmission system is illustrated. A mathematical model of EW fading channel for FSO is developed in same section. Section 3 is devoted for mathematical analysis of FSO systems over EW fading channels considering fog and beam divergence. In Section 4, BER expressions of the LQAM-MPPM/FSO transmission system, considering fading and pointing-error, are derived. Our numerical results are given in Section 5, where the obtained BER expressions are used to investigate proposed system performance under different weather conditions, fading levels, and pointing-error. Finally, the conclusion is given in Section 6.

2. *LQAM-MPPM/FSO system and FSO channel model*

In this section, we describe in details the setup block diagram and operation of LQAM-MPPM/FSO transmission system. In addition, we develop a mathematical model for EW distribution in FSO transmission channels.

2.1. *LQAM-MPPM system setup*

The basic schematic block diagrams of both the transmitter and receiver of an LQAM-MPPM scheme are shown in Fig. 1. At the transmitter side, a frame of $\left\lfloor \log_2 \binom{N}{w} \right\rfloor + wm$ bits is fed to the transmitter signal-processing unit (T-SPU), where $\lfloor x \rfloor$ is the floor integer of x, and N and w are the number of MPPM time-slots and signal time-slots, respectively. $m = \log_2(L)$, where L is the cardinality of the constellation of LQAM technique. The T-SPU manipulates these bits to control the operation of both LQAM and DC-Bias level. $\left\lfloor \log_2 \binom{N}{w} \right\rfloor$ (MPPM data-word part) bits are manipulated to define the position of w signal-slots in N time-slots frame length. This control signal will control the ON and OFF operation of both the DC-Bias and the LQAM modulator. This data manipulation produces a control signal that decodes wm bits (LQAM data-word part) in the w signal time-slots. The output of the LQAM modulator is added to the output of DC-biasing source and used to lighten up the laser diode (LD). This output optical signal power for the ith time-slot is expressed as:

$$P_i(t) = \frac{N}{w} \hat{P} \left[1 + M D_i(t)\right] B_i(t) \operatorname{rect}_\tau (t - i\tau), \tag{1}$$

where $\hat{P}$ is the average launch optical power, $\frac{N}{w}\hat{P}$ is the instantaneous transmitted optical power in signal time-slot, M is the modulation-index, and τ is the time-slot duration. $D_i(t)$ is the LQAM symbol which consists of both in-phase, r_I, and quadrature-phase, r_Q, signal components around a carrier frequency of f_c [25]. $B_i(t) = 1$ for signal time-slots, while for non-signal time-slots $D_i(t) = B_i(t) = 0$, and $\operatorname{rect}(\cdot)$ is the rectangular function, defined as:

$$\operatorname{rect}_\tau(t) \stackrel{\text{def}}{=} \begin{cases} 1; & 0 \le t \le \tau, \\ 0; & \text{otherwise}. \end{cases} \tag{2}$$

This optical signal is directed through FSO channel and suffers from both scintillation and fog effects. At the receiver side, the output current of the photodetector (PD) can be written as:

$$y_i(t) = I_{ph}(t) \left[1 + M D_i(t)\right] B_i(t) \operatorname{rect}_\tau (t - i\tau) + n(t), \tag{3}$$

where $n(t)$ is Gaussian noise with variance σ_n^2 and $I_{ph}(t) = (N/w)\mathcal{R}\hat{P}H$. Here, $\mathcal{R}$ denotes the photodiode's responsivity and H denotes the FSO channel response. This output signal is band-limited using a band-pass filter (BPF) to remove the out-band noise and distortion in order to improve the required received signal quality. Next, the band-limited signal is fed into two arms through the 3 dB coupler.

On the upper-arm (MPPM demodulator), the signal is integrated over each time slot, τ, and fed to the receiver signal-processing unit (R-SPU). In R-SPU, the output of the integrator is digitized, using analog-to-digital converter (ADC), and stored. The N stored levels are sorted in a descending order to decide the w highest-levels which are corresponding to the signal time-slots of the MPPM symbol. After that, the R-SPU decodes the MPPM symbols based on MPPM symbols-to-bits map.

On the other-arm (LQAM demodulator), the decoding of the LQAM data is performed after a fixed delay-line of two-frames time duration. This delay introduces sufficient time for the R-SPU to determine the position of the w highest level time-slots. These w time-slots contain the w LQAM symbols. The mixers with low-pass filters (LPFs) are used to obtain the in-phase, r_I, and quadrature-phase, r_Q, signal components. Then, the positions of w highest-level time-slots determine the expected time-slots to find LQAM symbols. After that, the R-SPU decodes the selected LQAM symbols based on LQAM symbols-to-bits map. Finally, the received data words are reconstructed from the decoded MPPM and LQAM bits.

2.2. *FSO transmission channel model*

According to [9], the turbulence gain h is well described by exponentiated Weibull (EW) distribution, where its probability density function
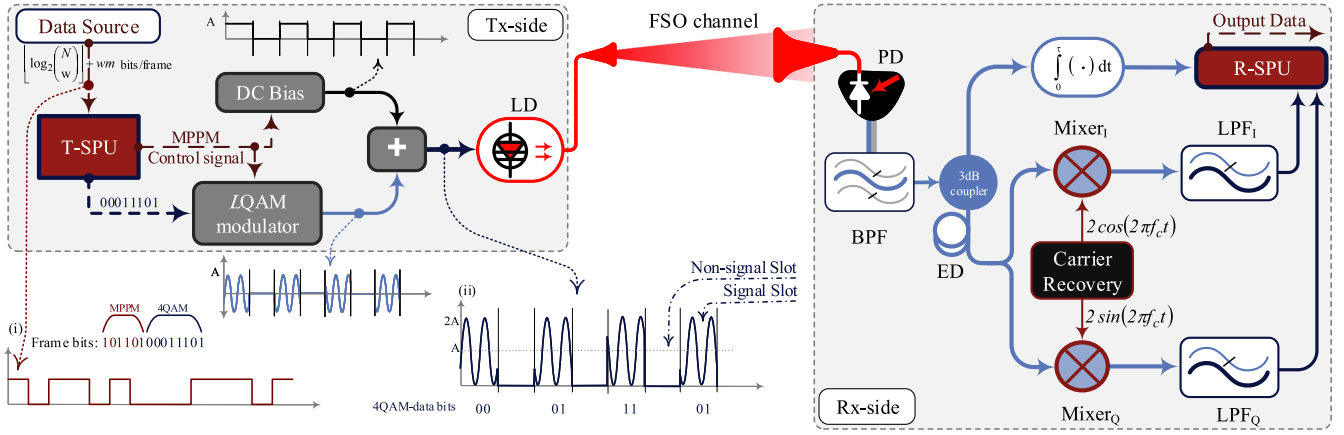
Fig. 1. Block diagram of FSO transmission system adopting $LQAM$-MPPM modulation technique. LD: Laser Diode, PD: Photo Detector, LPF: Low Pass Filter, BPF: Band Pass Filter, ED: Electronic Delay, DC: Direct Current, I: I- channel signal, Q: Q channel signal, T(R)-SPU: Transmitter (Receiver) Signal Processing Unit. The time domain signal sketch (*ii*) of a transmitted $LQAM$-MPPM frame with ($L = 4$, $N = 8$ and $w = 4$) and (*i*) is the bits stream in one frame.

(pdf) and cumulative distribution function (CDF) are given as follows:

$$f_h(h; \beta, \eta, \alpha) = \frac{\alpha\beta}{\eta} \left(\frac{h}{\eta}\right)^{\beta-1} \exp\left(-\left(\frac{h}{\eta}\right)^{\beta}\right)$$
$$\times \left[1 - \exp\left(-\left(\frac{h}{\eta}\right)^{\beta}\right)\right]^{\alpha-1}, \tag{4}$$

$$F_h(h; \beta, \eta, \alpha) = \left[1 - \exp\left(-\left(\frac{h}{\eta}\right)^{\beta}\right)\right]^{\alpha}, \tag{5}$$

respectively, where $\alpha > 0$ is an extra shape parameter that is strongly dependent on the receiver aperture size, $\beta > 0$ is a shape parameter that is related to the scintillation index σ_I^2, and $\eta > 0$ is a scale parameter that depends on both α and β. The expressions for α, β, and η are given as [26]:

$$\alpha \approx 3.931 \left(\frac{D_R}{\rho_o}\right)^{-0.519}, \beta \approx \left(\alpha\sigma_I^2\right)^{\frac{-6}{11}}, \eta = \frac{1}{\alpha\Gamma(1 + \frac{1}{\beta})g(\alpha, \beta)}, \tag{6}$$

respectively, where $\rho_o = (1.46C_n^2(2\pi/\lambda)^2 L_p)^{-3/5}$ is the atmospheric coherence radius, λ is the transmission wavelength, L_p is the FSO link length, C_n^2 is the refractive-index structure constant. Furthermore, D_R is the aperture diameter, $\Gamma(\cdot)$ is the gamma function and $g(\alpha, \beta)$ is defined as:

$$g(\alpha, \beta) = \sum_{i=0}^{\infty} \frac{(-1)^i (i+1)^{-(1+\beta)/\beta}\Gamma(\alpha)}{i!\Gamma(\alpha - i)}. \tag{7}$$

3. Performance analysis considering fog and beam divergence

The FSO channel response H includes different weather effects such as turbulence gain h, fog attenuation, and beam divergence attenuation. It can be expressed as:

$$H = \xi h, \tag{8}$$

where $\xi = \xi_n(L_p)/\xi_d(L_p)$ is the normalized path-loss coefficient with respect to the path-loss of direct link in clear weather conditions $\xi_d(L_p)$. $\xi_n(L_p) = 10^{-(UL_p/10)}[D_R^2/(D_T + \theta_T L_p)^2]$, where D_R and D_T are the receiver and transmitter aperture diameters, respectively, U is the weather dependent attenuation coefficient (in dB/km), and θ_T is the optical beam-divergence angle (in mrad). It is clear that $\xi_n(L_p)$ is calculated by combining weather attenuation with geometric losses [27–29]. Furthermore, the instantaneous signal-to-noise ratio γ, including channel effects, can be defined as [30]:

$$\gamma = \left(\frac{N}{w}\right)^2 \frac{(\hat{P}\mathcal{R})^2}{\sigma_n^2} H^2 = \left(\frac{N}{w}\right)^2 H^2 \hat{\gamma}, \tag{9}$$

where $\hat{\gamma}$ is the average signal-to-noise ratio (SNR). By making simple transformation of the random variable in both (4) and (5), we get the pdf and CDF expressions of γ as follows:

$$f_\gamma(\gamma; \beta, \eta, \alpha) = \frac{\alpha\beta}{2\gamma} \left(\frac{(w/N)^2}{\hat{\gamma}\eta^2\xi^2}\gamma\right)^{\frac{\beta}{2}} \exp\left(-\left(\frac{(w/N)^2}{\hat{\gamma}\eta^2\xi^2}\gamma\right)^{\frac{\beta}{2}}\right)$$
$$\times \left[1 - \exp\left(-\left(\frac{(w/N)^2}{\hat{\gamma}\eta^2\xi^2}\gamma\right)^{\frac{\beta}{2}}\right)\right]^{\alpha-1}, \tag{10}$$

$$F_\gamma(\gamma; \beta, \eta, \alpha) = \left[1 - \exp\left(-\left(\frac{(w/N)^2}{\hat{\gamma}\eta^2\xi^2}\gamma\right)^{\frac{\beta}{2}}\right)\right]^{\alpha}, \tag{11}$$

respectively. By applying Newton's generalized-binomial theorem [31]:

$$(1 + z)^r = \sum_{j=0}^{\infty} \frac{\Gamma(r+1)z^j}{j!\Gamma(r-j+1)} \tag{12}$$

and expressing the exponential function in terms of MeijerG function [32], where $\exp(x) = G_{0,1}^{1,0}\left(-x \Big|_0^{-}\right)$, the last pdf and CDF expressions can be written as:

$$f_\gamma(\gamma; \beta, \eta, \alpha) = \frac{\alpha\beta\Gamma(\alpha)\gamma^{(\frac{\beta}{2}-1)}}{2\left((N/w)^2\hat{\gamma}\eta^2\xi^2\right)^{\frac{\beta}{2}}} \sum_{j=0}^{\infty} \frac{(-1)^j}{j!\Gamma(\alpha - j)}$$
$$\times G_{0,1}^{1,0}\left((1+j)\left(\frac{(w/N)^2}{\hat{\gamma}\eta^2\xi^2}\gamma\right)^{\frac{\beta}{2}} \Big|_0^{-}\right), \tag{13}$$

$$F_\gamma(\gamma; \beta, \eta, \alpha) = \Gamma(\alpha+1) \sum_{j=0}^{\infty} \frac{(-1)^j}{j!\Gamma(\alpha - j + 1)} G_{0,1}^{1,0}\left(j\left(\frac{(w/N)^2}{\hat{\gamma}\eta^2\xi^2}\gamma\right)^{\frac{\beta}{2}} \Big|_0^{-}\right), \tag{14}$$

respectively.

3.1. BER expressions

The BER of the $LQAM$-MPPM scheme is the average of the BERs of both $LQAM$ and MPPM schemes and is given as [10]:

$$\text{BER} = \frac{\log_2\binom{N}{w}}{\log_2\binom{N}{w} + wm} \text{BER}_{\text{MPPM}} + \frac{wm}{\log_2\binom{N}{w} + wm}$$
$$\times \left(\text{BER}_{LQAM}\left(1 - \text{SER}_{\text{MPPM}}\right) + \frac{\text{SER}_{\text{MPPM}}}{2}\right), \tag{15}$$

where BER_{LQAM} is the bit-error rate of ordinary $LQAM$ and SER_{MPPM} is the symbol-error rate of the ordinary MPPM scheme. The first term in (15) accounts for bit-error rate that occurs in the group of $\left\lfloor \log_2\binom{N}{w}\right\rfloor$

bits transmitted using MPPM. The second term represents the bit-error rate of the remaining wm bits and it consists of two parts. The first part considers the case when the MPPM signal-slots are correctly decoded, while the other part considers the case of incorrect decoding of MPPM signal-slots. The SER_{MPPM} and BER_{LQAM} are given as [2,17]:

$$\text{SER}_{\text{MPPM}}(\gamma) \leq \frac{\binom{N}{w} - 1}{2} \operatorname{erfc}\left(\sqrt{\frac{\gamma}{4N} \log_2\binom{N}{w}}\right),\tag{16}$$

$$\text{BER}_{LQAM}(\gamma) = \frac{2}{m}$$

$$\times \begin{cases} \left(1 - \frac{1}{\sqrt{L}}\right) \sum_{i=1}^{\sqrt{L}/2} \operatorname{erfc}\left((2i-1)\sqrt{\frac{3M^2\gamma}{4(L-1)}}\right); & \text{for even } m, \\ \operatorname{erfc}\left(\sqrt{\frac{3M^2\gamma}{4(L-1)}}\right); & \text{for odd } m, \end{cases}\tag{17}$$

respectively. Furthermore, the relation between BER_{MPPM} and SER_{MPPM} is given as [24]:

$$\text{BER}_{\text{MPPM}} \leq \frac{(2)^{\left\lfloor \log_2\binom{N}{w} \right\rfloor - 1}}{(2)^{\left\lfloor \log_2\binom{N}{w} \right\rfloor} - 1} \text{SER}_{\text{MPPM}}.\tag{18}$$

The next subsections are devoted for obtaining upper bound and approximate upper bound expressions for both BER_{LQAM} and SER_{MPPM} under EW fading FSO channel in order to evaluate the overall BER of (15) over turbulent FSO transmission channel.

3.2. Upper bound BER expressions

In this subsection, an expression for the upper bound BER of $LQAM$-MPPM scheme is derived based on MeijerG function. Using $\operatorname{erfc}(x) = \frac{1}{\sqrt{\pi}} \text{G}_{1,2}^{2,0}\left(x^2 \Big|_{0, 0.5}^{1}\right)$ [32], the SER_{MPPM} in (16) can be rewritten as follows:

$$\text{SER}_{\text{MPPM}}(\gamma) \leq \frac{\binom{N}{w} - 1}{2\sqrt{\pi}} \text{G}_{1,2}^{2,0}\left(\frac{\gamma \log_2\binom{N}{w}}{4N} \Big|_{0, 0.5}^{1}\right).\tag{19}$$

The average SER is obtained by averaging of $\text{SER}_{\text{MPPM}}(\gamma)$ in (19) over the pdf in (13) with respect to the instantaneous signal-to-noise ratio γ. Thus, based on the general integration form of the MeijerG function [32], the average SER_{MPPM} is obtained by:

$$\text{SER}_{\text{MPPM}} = \int_0^\infty \text{SER}_{\text{MPPM}}(\gamma) f_\gamma(\gamma; \beta, \eta, \alpha)d\gamma,\tag{20}$$

$$\text{SER}_{\text{MPPM}} \leq \left(\binom{N}{w} - 1\right) \frac{\alpha\beta\Gamma(\alpha)(w/N)^\beta}{4\sqrt{\pi}\left(\hat{\gamma}\eta^2\xi^2\right)^{\frac{\beta}{2}}} \sum_{j=0}^\infty \frac{(-1)^j}{j!\Gamma(\alpha - j)}$$

$$\times \int_0^\infty \gamma^{(\frac{\beta}{2} - 1)} \text{G}_{1,2}^{2,0}\left(\frac{\gamma \log_2\binom{N}{w}}{4N} \Big|_{0, 0.5}^{1}\right)$$

$$\times \text{G}_{0,1}^{1,0}\left((1+j)\left(\frac{\gamma}{\hat{\gamma}\eta^2\xi^2}\right)^{\frac{\beta}{2}} \Big|_0^{-}\right) d\gamma.\tag{21}$$

Thus, closed-form expression for the SER_{MPPM} is expressed as (22) in Box I where l and k are integers with $\frac{l}{k} = \frac{\beta}{2}$ and $\Delta(b, a) = \frac{a}{b}, \frac{a+1}{b}, \dots, \frac{a+b-1}{b}$. Similarly, by expressing the $\operatorname{erfc}(\cdot)$ in (17) with MeijerG function expression and averaging the result expression of $\text{BER}_{LQAM}(\gamma)$ over the pdf in (13) with respect to the instantaneous signal-to-noise ratio γ, average BER_{LQAM} of $LQAM$ scheme can be expressed as (23) in Box I.

The average BER of the hybrid $LQAM$-MPPM scheme under EW fading FSO channel considering both fog and beam divergence attenuations can be evaluated by substituting (22) and (23) in (15).

3.3. Approximate BER expressions

Due to the computation complexity of upper bound BER expressions obtained in previous subsection, Gauss–Laguerre quadrature rule is used to get low-computational approximate expressions for average BER of hybrid $LQAM$-MPPM scheme. First, we express the average of $\text{SER}_{\text{MPPM}}(\gamma)$ as follows [33]:

$$\text{SER}_{\text{MPPM}} = -\int_0^\infty \frac{d\,\text{SER}_{\text{MPPM}}(\gamma)}{d\gamma} F_\gamma(\gamma; \beta, \eta, \alpha)d\gamma,\tag{24}$$

$$\text{SER}_{\text{MPPM}} \leq \int_0^\infty \frac{\left(\binom{N}{w} - 1\right)}{4} \sqrt{\frac{\log_2\binom{N}{w}}{\pi\gamma N}} \exp\left(-\frac{\gamma \log_2\binom{N}{w}}{4N}\right)$$

$$\times \left[1 - \exp\left(-\left(\frac{(w/N)^2}{\hat{\gamma}\eta^2\xi^2}\gamma\right)^{\frac{\beta}{2}}\right)\right]^\alpha d\gamma.\tag{25}$$

By performing change of variable $z = \gamma \log_2\binom{N}{w}/(4N)$, (25) can be rewritten as:

$$\text{SER}_{\text{MPPM}} \leq \int_0^\infty \frac{\left(\binom{N}{w} - 1\right)}{2\sqrt{\pi z}} \exp(-z)$$

$$\times \left[1 - \exp\left(-\left(\frac{4N(w/N)^2}{\hat{\gamma}\eta^2\xi^2\log_2\binom{N}{w}}z\right)^{\frac{\beta}{2}}\right)\right]^\alpha dz.\tag{26}$$

Using generalized Gauss–Laguerre quadrature rule [34], (26) can be accurately approximated in the form of a truncated series:

$$\text{SER}_{\text{MPPM}} \leq \sum_{i=1}^S \frac{\left(\binom{N}{w} - 1\right)}{2\sqrt{\pi V_i}} \Lambda_i$$

$$\times \left[1 - \exp\left(-\left(\frac{4N(w/N)^2}{\hat{\gamma}\eta^2\xi^2\log_2\binom{N}{w}}V_i\right)^{\frac{\beta}{2}}\right)\right]^\alpha,\tag{27}$$

where $S > 1$ denotes the number of terms, and for any $i \in \{1, 2, \dots, S\}$, V_i is the ith root of Laguerre polynomial $L_S(X)$ with degree S, and Λ_i is the corresponding weighting coefficient. Applying the same procedure, an approximate expression for the average $\text{BER}_{LQAM}(\gamma)$, with respect to instantaneous signal-to-noise ratio γ, can be obtained as (28) in Box II. Finally, approximate expression for $\text{BER}_{LQAM\text{-MPPM}}$ of the hybrid scheme is formulated by substituting (27) and (28) in (15).

4. Performance analysis considering pointing-error

In last section, both upper bound and approximate upper bound expressions have been derived for average BER of an IM/DD FSO system adopting hybrid $LQAM$-MPPM technique under exponentiated Weibull fading channels considering attenuations due to fog and beam divergence. In this section, the BER analysis is extended to include the impact of pointing-error (misalignment) under exponentiated Weibull turbulence. Neglecting path loss, the channel response H is composed of two independent random processes, namely, the pointing-error h_p and atmospheric turbulence fading h. That is, $H = hh_p$. The pointing-error h_p has been modeled as the result of considering independent identical Gaussian distributions, with variance σ_s^2, for both the elevation and horizontal displacement [26]. Therefore, the statistical model of the pointing-error fading is assumed to be [4,26]:

$$f_{h_p}(h_p) = \frac{\delta^2}{A_o^{\delta^2}} h_p^{\delta^2 - 1}; \qquad 0 \leq h_p \leq A_o,\tag{29}$$

where $A_o = (\operatorname{erf}(v))^2$, $v^2 = \frac{\pi a^2}{2W_b^2}$, a is the radius of the receiver, W_b is the beam radius at the receiver plane, and $\delta = \frac{W_{b_{eq}}}{2\sigma_s}$ is the ratio between the equivalent beam radius and the pointing-error jitter at the receiver, with $W_{b_{eq}}^2 = \frac{\sqrt{\pi}W_b^2 \operatorname{erf}(v)}{2v\exp(-v^2)}$. By applying the standard statistical procedures, the statistical distribution of the overall channel response, $f_H(H)$, is

Box I.

$$
\text{SER}_{\text{MPPM}} \le \left(\binom{N}{w} - 1 \right) \left(\frac{4N(w/N)^2}{\hat{\gamma}\log_2\binom{N}{w}\eta^2\xi^2} \right)^{\frac{\beta}{2}} \frac{\alpha\beta\Gamma(\alpha)k^{0.5}l^{(\frac{\beta}{2}-1)}}{4\sqrt{\pi}(2\pi)^{0.5(l+k)-1}} \sum_{j=0}^{\infty} \frac{(-1)^j}{j!\,\Gamma(\alpha-j)} \text{G}_{2l,k+l}^{k,2l} \left(\left(\frac{1+j}{k}\right)^k \left(\frac{4(w/N)^2Nl}{\log_2\binom{N}{w}\hat{\gamma}\eta^2\xi^2}\right)^l \Bigg|_{\Delta(k,0),\ \Delta(l,-\frac{\beta}{2})}^{\Delta(l,1-\frac{\beta}{2}),\ \Delta(l,0.5-\frac{\beta}{2})} \right),
\tag{22}
$$

$$
\text{BER}_{LQAM} = \frac{k^{0.5}l^{(\frac{\beta}{2}-1)}\alpha\beta\Gamma(\alpha)}{m\sqrt{\pi}(2\pi)^{0.5(l+k)-1}} \left(\frac{4(w/N)^2(L-1)}{3\hat{\gamma}\eta^2\xi^2M^2} \right)^{\frac{\beta}{2}} \sum_{j=0}^{\infty} \frac{(-1)^j}{j!\,\Gamma(\alpha-j)}
$$

$$
\times \begin{cases}
\displaystyle\sum_{i=1}^{\sqrt{L}/2} \frac{1}{(2i-1)^{\beta}} \text{G}_{2l,k+l}^{k,2l}\left(\left(\frac{1+j}{k}\right)^k \left(\frac{4(w/N)^2(L-1)l}{3(2i-1)^2\hat{\gamma}\eta^2\xi^2M^2}\right)^l \Bigg|_{\Delta(k,0),\ \Delta(l,-\frac{\beta}{2})}^{\Delta(l,1-\frac{\beta}{2}),\ \Delta(l,0.5-\frac{\beta}{2})} \right); & \text{for even } m, \\[3ex]
\text{G}_{2l,k+l}^{k,2l}\left(\left(\frac{1+j}{k}\right)^k \left(\frac{4(w/N)^2(L-1)l}{3\hat{\gamma}\eta^2\xi^2M^2}\right)^l \Bigg|_{\Delta(k,0),\ \Delta(l,-\frac{\beta}{2})}^{\Delta(l,1-\frac{\beta}{2}),\ \Delta(l,0.5-\frac{\beta}{2})} \right); & \text{for odd } m.
\end{cases}
\tag{23}
$$

Box I.

Box II.

$$
\text{BER}_{LQAM} = \frac{2}{m\sqrt{\pi}} \sum_{j=1}^{S} \frac{\Lambda_j}{\sqrt{V_j}}
\begin{cases}
\left(1-\frac{1}{\sqrt{L}}\right)\displaystyle\sum_{i=1}^{\sqrt{L}/2}\left[1-\exp\left(-\left(\frac{4(L-1)(w/N)^2}{3M^2(2i-1)^2\hat{\gamma}\eta^2\xi^2}V_j\right)^{\frac{\beta}{2}}\right)\right]^{\alpha}, & \text{for even } m, \\[3ex]
\left[1-\exp\left(-\left(\frac{4(L-1)(w/N)^2}{3M^2\hat{\gamma}\eta^2\xi^2}V_j\right)^{\frac{\beta}{2}}\right)\right]^{\alpha}, & \text{for odd } m.
\end{cases}
\tag{28}
$$

Box II.

given as a conditional random process given a turbulence state h [26], as follows:

$$
f_H(H) = \frac{\delta^2}{A_o^2} H^{\delta^2-1} \int_{H/A_o}^{\infty} h^{-\delta^2} f_h(h;\beta,\eta,\alpha)\mathrm{d}h.
\tag{30}
$$

By applying Newton's generalized-binomial theorem in (4) and substituting in (30), we get:

$$
f_H(H) = \frac{\delta^2\alpha\beta\Gamma(\alpha)}{A_o^{\delta^2}\eta^{\beta}} H^{\delta^2-1} \sum_{j=0}^{\infty} \frac{(-1)^j}{j!\,\Gamma(\alpha-j)}
$$
$$
\times \int_{H/A_o}^{\infty} h^{\beta-\delta^2-1}\exp\left(-(1+j)\left(\frac{h}{\eta}\right)^{\beta}\right)\mathrm{d}h.
\tag{31}
$$

By performing change of variable, $y = h^{\beta}$ and using the integration form given in [35], the pdf of the overall response H is expressed as:

$$
f_H(H) = \frac{\delta^2\alpha\Gamma(\alpha)}{A_o^{\delta^2}\eta^{\delta^2}} H^{\delta^2-1} \sum_{j=0}^{\infty} \frac{(-1)^j(1+j)^{\frac{\delta^2}{\beta}-1}}{j!\,\Gamma(\alpha-j)}
$$
$$
\times \Gamma\left(1-\frac{\delta^2}{\beta},(1+j)\left(\frac{H}{\eta A_o}\right)^{\beta}\right),
\tag{32}
$$

where $\Gamma(\cdot,\cdot)$ is the upper-incomplete gamma function, which can be expressed in terms of the MeijerG function as: $\Gamma(a,x) = \text{G}_{1,2}^{2,0}\left(x\Big|_{0,\ a}^{1}\right)$ [32]. Therefore, (32) can be written as:

$$
f_H(H) = \frac{\delta^2\alpha\Gamma(\alpha)}{A_o^{\delta^2}\eta^{\delta^2}} H^{\delta^2-1} \sum_{j=0}^{\infty} \frac{(-1)^j(1+j)^{\frac{\delta^2}{\beta}-1}}{j!\,\Gamma(\alpha-j)}
$$
$$
\times \text{G}_{1,2}^{2,0}\left((1+j)\left(\frac{G}{\eta A_o}\right)^{\beta}\Bigg|_{0,\ 1-\frac{\delta^2}{\beta}}^{1}\right).
\tag{33}
$$

The CDF expression of the channel response $F_H(H)$ is formulated as [36]:

$$
F_H(H) = \frac{\delta^2\alpha\Gamma(\alpha)}{\beta A_o^{\delta^2}\eta^{\delta^2}} H^{\delta^2} \sum_{j=0}^{\infty} \frac{(-1)^j(1+j)^{\frac{\delta^2}{\beta}-1}}{j!\,\Gamma(\alpha-j)}
$$

$$
\times \text{G}_{2,3}^{2,1}\left((1+j)\left(\frac{H}{\eta A_o}\right)^{\beta}\Bigg|_{0,\ 1-\frac{\delta^2}{\beta},\ -\frac{\delta^2}{\beta}}^{1-\frac{\delta^2}{\beta},\ 1}\right).
\tag{34}
$$

Using (9), (19), and (34), we get the average of SER_{MPPM} using the CDF expression of the channel response $F_H(H)$ as follows:

$$
\text{SER}_{\text{MPPM}} = -\int_0^{\infty} \frac{\mathrm{d}\,\text{SER}_{\text{MPPM}}(H)}{\mathrm{d}H} F_H(H)\mathrm{d}H
\tag{35}
$$

$$
\text{SER}_{\text{MPPM}} \le \left(\binom{N}{w}-1\right)\sum_{j=0}^{\infty} \frac{(-1)^j(1+j)^{\frac{\delta^2}{\beta}-1}}{j!\,\Gamma(\alpha-j)}
$$

$$
\times \frac{\delta^2\alpha\Gamma(\alpha)}{\sqrt{\pi}\beta A_o^{\delta^2}\eta^{\delta^2}} \int_0^{\infty} \exp\left(\frac{-\bar{\gamma}\left(\frac{N}{w}\right)^2\log_2\binom{N}{w}}{4N}H^2\right)
$$

$$
\times H^{\delta^2}\text{G}_{2,3}^{2,1}\left((1+j)\left(\frac{H}{\eta A_o}\right)^{\beta}\Bigg|_{0,\ 1-\frac{\delta^2}{\beta},\ -\frac{\delta^2}{\beta}}^{1-\frac{\delta^2}{\beta},\ 1}\right)\mathrm{d}H.
\tag{36}
$$

Using similar analysis to that explored in Section 3.3, we substitute $z = \frac{\hat{\gamma}\left(\frac{N}{w}\right)^2\log_2\binom{N}{w}}{4N}H^2$ and rewrite (36) as:

$$
\text{SER}_{\text{MPPM}} \le \left(\binom{N}{w}-1\right)\left(\frac{4N}{\hat{\gamma}\left(\frac{N}{w}\right)^2\log_2\binom{N}{w}A_o^2\eta^2}\right)^{\frac{\delta^2}{2}} \frac{\delta^2\alpha\Gamma(\alpha)}{2\sqrt{\pi}\beta}
$$

$$
\times \sum_{j=0}^{\infty} \frac{(-1)^j(1+j)^{\frac{\delta^2}{\beta}-1}}{j!\,\Gamma(\alpha-j)} \int_0^{\infty} (z)^{\frac{\delta^2}{2}-\frac{1}{2}}\exp(-z)
$$

$$
\times \text{G}_{2,3}^{2,1}\left((1+j)\left(\frac{4N}{\hat{\gamma}\left(\frac{N}{w}\right)^2\log_2\binom{N}{w}\eta^2 A_o^2}z\right)^{\frac{\beta}{2}}\Bigg|_{0,\ 1-\frac{\delta^2}{\beta},\ -\frac{\delta^2}{\beta}}^{1-\frac{\delta^2}{\beta},\ 1}\right)\mathrm{d}z.
\tag{37}
$$

Based on generalized Gauss–Laguerre quadrature rule [34], the approximate expression for the average SER of MPPM scheme is given as (38) in Box III. Furthermore, an approximate expression for average BER of

$$\text{SER}_{\text{MPPM}} \leq \left(\binom{N}{w} - 1 \right) \frac{\delta^2 \alpha \Gamma(\alpha)}{2\sqrt{\pi}\beta} \left(\frac{4N(w/N)^2}{\hat{\gamma}\log_2\binom{N}{w}A_o^2\eta^2} \right)^{\frac{\delta^2}{2}} \sum_{j=0}^{\infty} \frac{(-1)^j(1+j)^{\frac{\delta^2}{\beta}-1}}{j!\Gamma(\alpha-j)} \sum_{i=1}^{S} \Lambda_i (V_i)^{\frac{\delta^2}{2}-\frac{1}{2}} G_{2,3}^{2,1} \left((1+j) \left(\frac{4N(w/N)^2}{\hat{\gamma}\log_2\binom{N}{w}\eta^2 A_o^2} V_i \right)^{\frac{\beta}{2}} \Big|_{0,\ 1-\frac{\delta^2}{\beta},\ -\frac{\delta^2}{\beta}}^{1-\frac{\delta^2}{\beta},\ 1} \right). \tag{38}$$

$$\text{BER}_{LQAM} = \frac{2\delta^2 \alpha \Gamma(\alpha)}{m\sqrt{\pi}\beta A_o^{\delta^2}\eta^{\delta^2}} \left(\frac{4(L-1)(w/N)^2}{3M^2\hat{\gamma}} \right)^{\frac{\delta^2}{2}+\frac{1}{2}} \sum_{j=0}^{\infty} \frac{(-1)^j(1+j)^{\frac{\delta^2}{\beta}-1}}{j!\Gamma(\alpha-j)} \sum_{r=1}^{S} \Lambda_r (V_r)^{\frac{\delta^2}{2}-\frac{1}{2}}$$
$$\times \begin{cases} \sum_{i=1}^{\sqrt{L}/2} \frac{1-\frac{1}{\sqrt{L}}}{(2i-1)^{\delta^2+1}} G_{2,3}^{2,1} \left((1+j) \left(\frac{4(L-1)(w/N)^2}{3M^2\hat{\gamma}(2i-1)^2\eta^2 A_o^2} V_r \right)^{\frac{\beta}{2}} \Big|_{0,\ 1-\frac{\delta^2}{\beta},\ -\frac{\delta^2}{\beta}}^{1-\frac{\delta^2}{\beta},\ 1} \right); & \text{for even } m, \\[2em] G_{2,3}^{2,1} \left((1+j) \left(\frac{4(L-1)(w/N)^2}{3M^2\hat{\gamma}\eta^2 A_o^2} V_r \right)^{\frac{\beta}{2}} \Big|_{0,\ 1-\frac{\delta^2}{\beta},\ -\frac{\delta^2}{\beta}}^{1-\frac{\delta^2}{\beta},\ 1} \right); & \text{for odd } m. \end{cases} \tag{39}$$

Box III.

$LQAM$ scheme can be derived using similar steps (see Appendix) to that used in case of MPPM that is expressed by (39) in Box III. Finally, by substituting (38) and (39) in (15), the average BER of hybrid $LQAM$-MPPM scheme considering fading and pointing-error can be evaluated.

5. Discussion and numerical results

In this section, the performance of FSO systems adopting $LQAM$-MPPM scheme is numerically evaluated using the expressions of the bit-error rates obtained in the previous sections. We consider FSO system performance under different turbulent levels, weather conditions, beam divergence, and pointing-error.

5.1. Upper bound and approximate BER expressions

Fig. 2 shows average BERs of hybrid $LQAM$-MPPM scheme (with $N = 4, w = 2$, and $L = 8$) versus average signal-to-noise SNR (in dB) under moderate turbulent, clear weather channels ($U = 0.19$ dB/km), and beam divergence of $\theta_T = 2$ mrad. Two different sets of receiver parameters are considered: ($D_R = 3$ mm; $\alpha = 5.44$, $\beta = 0.76$, $\eta = 0.31$), and ($D_R = 25$ mm; $\alpha = 4.65$, $\beta = 1.17$, $\eta = 0.52$). The modulation-index and operating wavelength are $M = 0.8$ and $\lambda = 780$ nm, respectively. Both upper bound and approximate upper bound expressions (with $S = 100$) are used in calculating the average BERs. It can be seen that for different FSO system parameters, the BER results of the upper bound expression are very tight to that of the approximate expression. Therefore, we use the approximate expression to calculate BERs in the next subsections as it has a lower computational complexity. In addition, Fig. 2 reveals that increasing receiver diameter leads to significant improvement in $LQAM$-MPPM/FSO system performance. This can be explained as follows. Increasing receiver aperture-diameter leads to receiving many off-axis components in addition to the on-axis direct beam. Therefore, the receiver averages the fluctuations of the received optical signals over its aperture. Thus, the fading effect is reduced by increasing the receiver aperture size. Specifically, at a BER of 10^{-3}, when using $D_R = 25$ mm, the system performance is improved by about 7 dB compared with that of $D_R = 3$ mm.

5.2. Hybrid versus ordinary schemes

The performance of FSO system adopting hybrid $LQAM$-MPPM/FSO is compared to that adopting ordinary MPPM and $LQAM$ schemes as shown in Figs. 3 and 4, respectively.

Modulation parameters (N, w and, L) are chosen so as to ensure that all systems under comparison have comparable transmission data rate, same average energy-per-bit, and bandwidth. In Fig. 3, we select hybrid $LQAM$-MPPM with ($N = 12, w = 2, L = 4$; 10 bits/symbol) and ordinary MPPM with ($N = 12, w = 5$; 9 bits/symbol). The same average
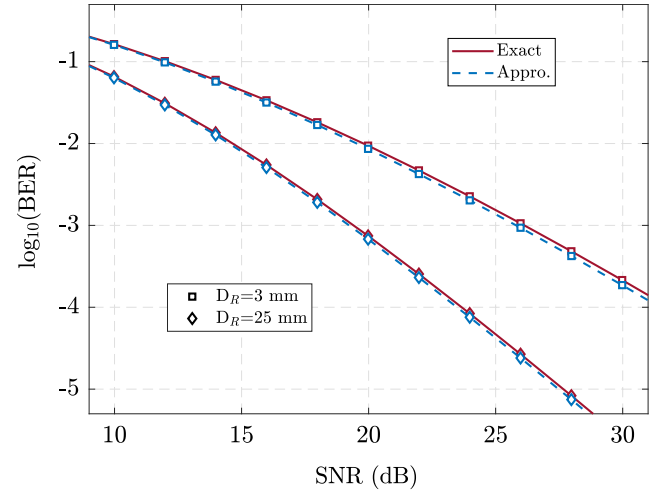

Fig. 2. Average bit-error rates (BERs) for hybrid $LQAM$-MPPM (with $N = 4, w = 2$, and $L = 8$) versus average signal-to-noise ratio over FSO channel with moderate fading and clear weather conditions: $U = 0.19$ dB/km and $\theta_T = 2$ mrad. The modulation-index of 8QAM is $M = 0.8$ and operating wavelength is $\lambda = 780$ nm.

power is considered for both schemes, so they have comparable data rate, energy per bit, and the same bandwidth. Three different aperture sizes are discussed. Specifically, ($D_R = 3$ mm; $\alpha = 5.44$, $\beta = 0.76$, $\eta = 0.31$), ($D_R = 60$ mm; $\alpha = 3.19$, $\beta = 2.61$, $\eta = 0.82$), and ($D_R = 80$ mm; $\alpha = 2.29$, $\beta = 4.84$, $\eta = 0.94$). While for Fig. 4, we select $LQAM$-MPPM with ($N = 4, w = 2, L = 8$; 8 bits/symbol) and ordinary $LQAM$ with ($L = 4$; 2 bits/symbol) and it will send 4 symbols during the hybrid scheme duration. Considering the same average power for both hybrid and ordinary $LQAM$ scheme, they have the same data rate, energy per bit, and the same bandwidth. Three different aperture sizes are discussed, ($D_R = 3$ mm; $\alpha = 5.44$, $\beta = 0.76$, $\eta = 0.31$), ($D_R = 25$ mm; $\alpha = 4.65$, $\beta = 1.17$, $\eta = 0.52$), and ($D_R = 80$ mm; $\alpha = 2.29$, $\beta = 4.84$, $\eta = 0.94$). It is concluded from figures that increasing aperture size improves the system performance through averaging the effect of turbulence over the aperture area for different modulation schemes. In addition, using hybrid $LQAM$-MPPM scheme improves FSO system performance when compared with both ordinary MPPM and $LQAM$ schemes. The reason behind this improvement is that when transmitting comparable data rates and same bandwidth at a specific average signal-to-noise ratio (specific average optical power), hybrid $LQAM$-MPPM systems have higher instantaneous signal-to-noise ratio as compared to corresponding ordinary $LQAM$ system and this leads to a reduction in the BERs of $LQAM$ part in hybrid scheme comparing
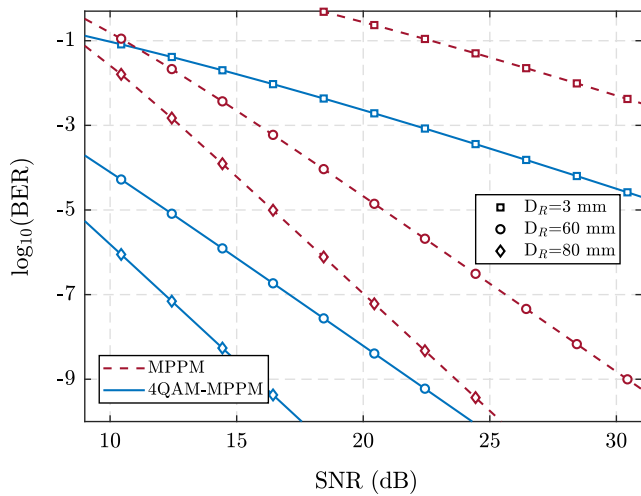
Fig. 3. Average bit-error rates for both hybrid LQAM-MPPM ($N = 12, w = 2$, and $L = 4$) and ordinary MPPM ($N = 12$ and $w = 5$) versus average signal-to-noise ratio over FSO channel with moderate fading and clear weather conditions: U =0.19 dB/km, θ_T =2 mrad, for different aperture sizes of D_R = 3, 60, and 80 mm. The modulation-index is $M = 0.8$ and operating wavelength is $\lambda = 780$ nm.
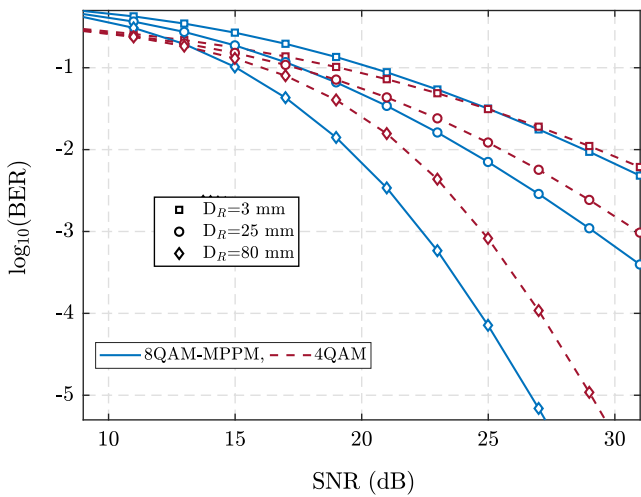

Fig. 5. Average bit-error rates for hybrid LQAM-MPPM ($N = 4$, $w = 2$, and $L = 8$) versus average signal-to-noise ratio over weak fading FSO channel with $\theta_T = 2$ mrad and different weather conditions; clear-, haze-, and thin-fog with $U = 0.24, 2.58, 4.22$ dB/km, respectively. The modulation-index is $M = 0.8$ and operating wavelength is $\lambda = 780$ nm.

Fig. 4. Average bit-error rates for both hybrid LQAM-MPPM ($N = 4, w = 2$, and $L = 8$) and ordinary LQAM ($L = 4$) versus average signal-to-noise ratio over FSO channel with moderate fading, haze: $U = 2.58$ dB/km, $\theta_T = 2$ mrad, for different aperture sizes of D_R = 3, 60, and 80 mm. The modulation-index is $M = 0.8$ and operating wavelength is $\lambda = 780$ nm.

it in ordinary LQAM scheme. Comparing to ordinary MPPM under the same conditions, ordinary MPPM increases the number of signal slots to increase number of bits per symbol in order to keep comparable data rate constrain. This leads to increasing in ordinary MPPM SER comparing that in hybrid scheme. Specifically, from Fig. 3, at a BER of 10^{-6}, the LQAM-MPPM based system outperforms ordinary MPPM based system by about 8 and 10 dB for D_R = 80 and 60 mm, respectively. Moreover, it can be seen from Fig. 4, when comparing LQAM-MPPM with ordinary LQAM, the hybrid scheme introduces a power saving by about 2 and 1 dB for D_R = 80 and 25 mm, respectively, at a BER of 10^{-3}.

5.3. Weather conditions effects

In Fig. 5, we investigate the effect of weather conditions on performance of FSO system adopting LQAM-MPPM scheme under weak
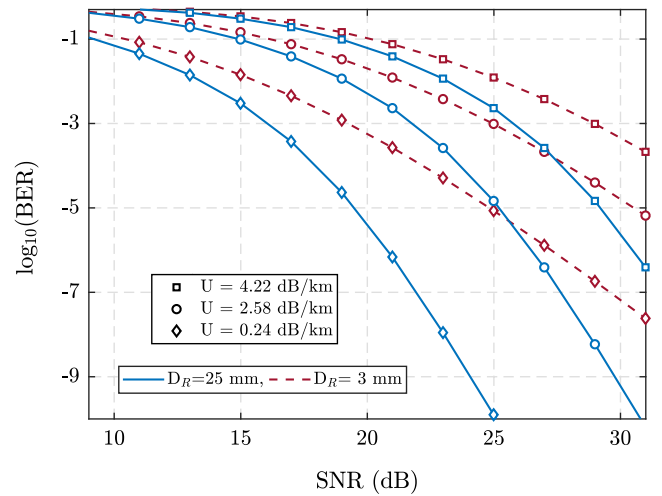
turbulent FSO transmission channel. Two aperture sizes are discussed: ($D_R = 3$ mm; $\alpha = 5.44$, $\beta = 1.78$, $\eta = 0.62$) and ($D_R = 25$ mm; $\alpha = 3.75$, $\beta = 5.44$, $\eta = 0.89$). We consider different weather conditions; clear-, haze-, and thin-fog with $U = 0.24, 2.58$, and 4.22 dB/km, respectively. It is shown that increasing aperture size provides an improvement in the FSO system performance even under bad weather conditions. This is because using larger aperture size means collecting more optical signal power and decreasing effective path loss. Specifically, the system using aperture size $D_R = 25$ mm outperforms that using $D_R = 3$ mm by about 6 dB at a BER of 10^{-6}, 6 dB at a BER of 10^{-4}, and 3.5 dB at a BER of 10^{-4} in case of clear-, haze-, and thing-fog weather, respectively.

5.4. Modulation-index effect

The effect of modulation-index M on the BERs performance is investigated in Fig. 6. We consider FSO system adopting hybrid LQAM-MPPM scheme (with $N = 4$, $w = 2$, and $L = 8$) under weak-turbulent channels (with $D_R = 25$ mm; $\alpha = 3.75$, $\beta = 5.44$, $\eta = 0.89$) and clear weather conditions (with $U = 0.19$ dB/km). As shown in Fig. 6, the BER performance of MPPM technique is constant for a given SNR and independent of the value of the modulation index, M, while increasing M improves the BER performance of LQAM technique. For $M < 0.4$, $\text{BER}_{LQAM} \gg \text{BER}_{MPPM}$ thus the performance of the LQAM is the dominant and the net average BER for the LQAM-MPPM system is improved with increasing M. This situation is reversed beyond a modulation index of 0.4, where $\text{BER}_{LQAM} \ll \text{BER}_{MPPM}$ and the average BER is dominated by the MPPM performance. Thus, the BER becomes approximately constant for $M \geq 0.4$. Based on the results, we can conclude that in order to get the optimal BER performance for FSO system adopting LQAM-MPPM scheme at different average signal-to-noise ratios, we should select a modulation-index with a value $M \geq 0.4$.

5.5. Pointing-error effect

Fig. 7 illustrates the impact of the pointing-error (PE) on the FSO system performance. The average BERs of hybrid LQAM-MPPM scheme (with $N = 8$, $w = 4$, and $L = 8$) under weak-turbulent FSO channel ($\sigma_R^2 = 0.32$) for two different aperture sizes: ($D_R = 50$ mm; $\alpha = 2.81$, $\beta = 3.31$, $\eta = 0.88$) and ($D_R = 200$ mm; $\alpha = 0.99$, $\beta = 20$, $\eta = $
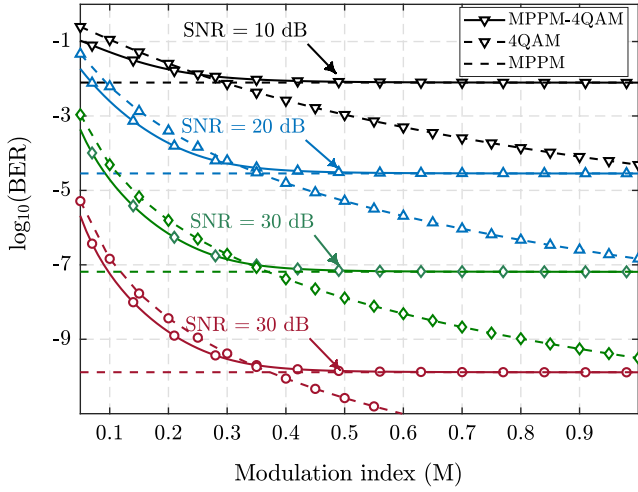
Fig. 6. Average bit-error rates for MPPM ($N = 4$, $w = 2$), 4QAM, and hybrid LQAM-MPPM ($N = 4$, $w = 2$, and $L = 4$) versus modulation-index M for different values of average signal-to-noise ratio, SNR, over clear weather conditions, $U = 0.19$ dB/km, $\theta_T = 2$ mrad, and aperture size of ($D_R = 25$ mm; $\alpha = 4.65$, $\beta = 1.17$, $\eta = 0.52$). The operating wavelength is $\lambda = 780$ nm.
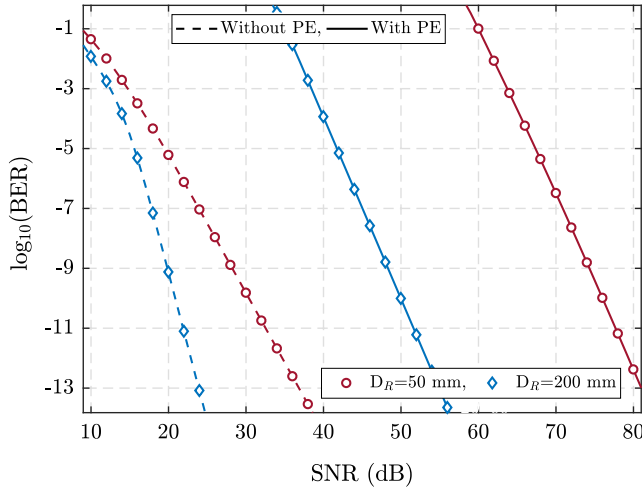

Fig. 7. Average bit-error rates for hybrid LQAM-MPPM ($N = 8$, $w = 4$, and $L = 8$) versus average signal-to-noise ratio over FSO channel for two different aperture sizes; ($D_R = 50$ mm; $\alpha = 2.81$, $\beta = 3.31$, $\eta = 0.88$), ($D_R = 200$ mm; $\alpha = 0.99$, $\beta = 20$, $\eta = 1.03$). The modulation-index is $M = 0.8$ and operating wavelength is $\lambda = 780$ nm.

1.03). Two cases are plotted: without pointing-error and with pointing-error ($\sigma_s = 0.3$ m). It is shown that the pointing-error highly degrades the FSO system performance. In addition, increasing the aperture size beats the degradation of the pointing-error on the system performance. Specifically, at a BER of 10^{-9}, for $D_R = 50$ mm, the system performance is degraded by about 45 dB, while for $D_R = 200$ mm it is degraded by only about 28 dB.

6. Conclusion

Closed-form expressions for upper bound of bit-error rates (BERs) have been derived for FSO system adopting hybrid LQAM-MPPM techniques under exponentiated Weibull (EW) fading channels. Upper bound BER expressions based on MeijerG function and approximate-tight expressions based on Gauss–Laguerre quadrature rule have been

derived considering fog and beam divergence. Furthermore, the mathematical analysis is extended to consider the pointing-error effect. In addition, the performance of FSO system adopting LQAM-MPPM has been compared to that adopting ordinary LQAM and MPPM schemes under different fading levels and weather conditions. It is revealed that the hybrid scheme performance outperforms that of ordinary techniques. In addition, the effect of modulation-index has been investigated. Finally, the pointing-error impact has been discussed and it has been found that the pointing-error introduces severe degradation in the FSO system performance; meanwhile the increase of receiver aperture size beats this performance degradation.

Appendix. Derivation of (39)

The average $\mathrm{BER}_{L\mathrm{QAM}}$ over EW channel response considering pointing-error can be obtained as:

$$\mathrm{BER}_{L\mathrm{QAM}} = -\int_0^\infty \frac{\mathrm{d}\,\mathrm{BER}_{L\mathrm{QAM}}(H)}{\mathrm{d}H} F_H(H)\mathrm{d}H. \tag{A.1}$$

By substituting of (9) in the $\mathrm{BER}_{L\mathrm{QAM}}(\gamma)$ expression (17), we get

$$\mathrm{BER}_{L\mathrm{QAM}}(H) = \frac{2}{m}$$

$$\times \begin{cases} \left(1 - \frac{1}{\sqrt{L}}\right) \sum_{i=1}^{\sqrt{L}/2} \mathrm{erfc}\left((2i-1)\left(\frac{N}{w}\right) M \sqrt{\frac{3\bar{\gamma}}{4(L-1)}} H\right); & \text{even } m, \\[2ex] \mathrm{erfc}\left(\left(\frac{N}{w}\right) M \sqrt{\frac{3\bar{\gamma}}{4(L-1)}} H\right); & \text{odd } m, \end{cases}$$

$$\tag{A.2}$$

$$\frac{\mathrm{d}\,\mathrm{BER}_{L\mathrm{QAM}}(H)}{\mathrm{d}H} = \frac{4}{m\sqrt{\pi}}\left(\frac{N}{w}\right) M \sqrt{\frac{3\bar{\gamma}}{4(L-1)}}$$

$$\times \begin{cases} \left(1 - \frac{1}{\sqrt{L}}\right) \sum_{i=1}^{\sqrt{L}/2} \exp\left((2i-1)\left(\frac{N}{w}\right) M \sqrt{\frac{3\bar{\gamma}}{4(L-1)}} H^2\right); & \text{even } m, \\[2ex] \exp\left(\left(\frac{N}{w}\right) M \sqrt{\frac{3\bar{\gamma}}{4(L-1)}} H^2\right); & \text{odd } m, \end{cases}$$

$$\tag{A.3}$$

By substituting in (A.1) with the CDF, $F_H(H)$, (34) and (A.3) for odd m case, we obtain

$$\mathrm{BER}_{L\mathrm{QAM}}^{\mathrm{odd}} = \frac{4}{m\sqrt{\pi}}\left(\frac{N}{w}\right) M \sqrt{\frac{3\bar{\gamma}}{4(L-1)}} \sum_{j=0}^\infty \frac{(-1)^j (1+j)^{\frac{\delta^2}{\beta}-1}}{j!\Gamma(\alpha-j)}$$

$$\times \frac{\delta^2 \alpha \Gamma(\alpha)}{\beta A_o^{\delta^2} \eta^{\delta^2}} \int_0^\infty \exp\left(-\left(\frac{N}{w}\right) M \sqrt{\frac{3\bar{\gamma}}{4(L-1)}} H^2\right)$$

$$\times H^{\delta^2} G_{2,3}^{2,1}\left((1+j)\left(\frac{H}{\eta A_o}\right)^\beta \left|\begin{matrix} 1-\frac{\delta^2}{\beta},\, 1 \\ 0,\, 1-\frac{\delta^2}{\beta},\, -\frac{\delta^2}{\beta} \end{matrix}\right.\right)\mathrm{d}H. \tag{A.4}$$

Using similar mathematical analysis that is explored in Section 3.3, we substitute $z = \frac{3\bar{\gamma}}{4(L-1)}\left(\frac{N}{w}\right)^2 M^2 H^2$ and rewrite (A.4) as:

$$\mathrm{BER}_{L\mathrm{QAM}}^{\mathrm{odd}} = \frac{2}{m\sqrt{\pi}} \sum_{j=0}^\infty \frac{(-1)^j (1+j)^{\frac{\delta^2}{\beta}-1}}{j!\Gamma(\alpha-j)} \frac{\delta^2 \alpha \Gamma(\alpha)}{\beta A_o^{\delta^2} \eta^{\delta^2}} \int_0^\infty (z)^{\frac{\delta^2}{2}-\frac{1}{2}}$$

$$\times \exp(-z) G_{2,3}^{2,1}\left((1+j)\left(\frac{4(L-1)}{3\bar{\gamma}\left(\frac{N}{w}\right)^2 M^2 \eta^2 A_o^2} z\right)^{\frac{\beta}{2}} \left|\begin{matrix} 1-\frac{\delta^2}{\beta},\, 1 \\ 0,\, 1-\frac{\delta^2}{\beta},\, -\frac{\delta^2}{\beta} \end{matrix}\right.\right)\mathrm{d}z. \tag{A.5}$$

Based on generalized Gauss–Laguerre quadrature rule [34].

$$\int_0^\infty (z-a)^c \exp(-b(z-a))f(z)\,\mathrm{d}z = \sum_{r=1}^S \Lambda_r f(V_r), \tag{A.6}$$

where $a = 0$, $c = 0$, $b = 1$, and $a = 0$. $S > 1$ denotes the number of terms, and for any $i \in \{1, 2, \dots, S\}$, V_i is the ith root of Laguerre polynomial $L_S(X)$ with degree S, and Λ_i is the corresponding weighting coefficient. $f(z)$ is expressed as

$$f(z) = (z)^{\frac{\delta^2}{2}-\frac{1}{2}} G_{2,3}^{2,1}\left((1+j)\left(\frac{4(L-1)}{3\hat{\gamma}\left(\frac{N}{w}\right)^2 M^2 \eta^2 A_o^2} z \right)^{\frac{\beta}{2}} \bigg|_{0,1-\frac{\delta^2}{\beta},-\frac{\delta^2}{\beta}}^{1-\frac{\delta^2}{\beta},1} \right). \tag{A.7}$$

Thus, the approximate expression for the average BER of LQAM scheme for odd m can be written as:

$$\mathrm{BER}_{LQAM}^{odd} = \frac{2\delta^2 \alpha \Gamma(\alpha)}{m\sqrt{\pi}\beta A_o^{\delta^2}\eta^{\delta^2}} \left(\frac{4(L-1)(w/N)^2}{3M^2\hat{\gamma}} \right)^{\frac{\delta^2}{2}+\frac{1}{2}}$$

$$\times \sum_{j=0}^\infty \frac{(-1)^j (1+j)^{\frac{\delta^2}{\beta}-1}}{j!\Gamma(\alpha-j)} \sum_{r=1}^S \Lambda_r (V_r)^{\frac{\delta^2}{2}-\frac{1}{2}}$$

$$\times G_{2,3}^{2,1}\left((1+j)\left(\frac{4(L-1)(w/N)^2}{3M^2\hat{\gamma}\eta^2 A_o^2} V_r \right)^{\frac{\beta}{2}} \bigg|_{0,\ 1-\frac{\delta^2}{\beta},\ -\frac{\delta^2}{\beta}}^{1-\frac{\delta^2}{\beta},\ 1} \right). \tag{A.8}$$

Also, the expression of $\mathrm{BER}_{LQAM}^{even}$ for even m case would be driven in similar way and the final expression of (39) is obtained.

References

[1] M.A. Khalighi, M. Uysal, Survey on free space optical communication: a communication theory perspective, IEEE Commun. Surv. Tutor. 16 (4) (2014) 2231–2258.

[2] A.E. Morra, H.S. Khallaf, H.M.H. Shalaby, Z. Kawasaki, Performance analysis of both shot- and thermal-noise limited multipulse PPM receivers in Gamma-Gamma atmospheric channels, IEEE/OSA J. Lightwave Technol. 31 (19) (2013) 3142–3150.

[3] M.A. Esmail, H. Fathallah, M.S. Alouini, Analysis of fog effects on terrestrial free space optical communication links, in: 2016 IEEE International Conference on Communication Workshops (ICC), no. 151–156, IEEE, 2016.

[4] A.A. Farid, S. Hranilovic, Outage capacity optimization for free-space optical links with pointing errors, IEEE/OSA J. Lightwave Technol. 2 (7) (2007) 1702–1710.

[5] F.S. Vetelino, C. Young, L. Andrews, Fade statistics and aperture averaging for Gaussian beam waves in moderate-to-strong turbulence, OSA Appl. Opt. 46 (18) (2007) 3780–3789.

[6] N. Perlot, D. Fritzsche, Aperture-averaging: theory and measurements, in: Proc. of SPIE, Vol. 5338, 2004, pp. 233–242.

[7] R.L. Al-Habash, M.A. Andrews, L.C. Phillips, Mathematical model for the irradiance probability density function of a laser beam propagating through turbulent media, Opt. Eng. 40 (8) (2001) 1554–1562.

[8] B. Epple, Simplified channel model for simulation of free-space optical communications, IEEE/OSA J. Opt. Commun. Networking 2 (5) (2010) 293–304.

[9] R. Barrios, F. Dios, Exponentiated Weibull distribution family under aperture averaging for Gaussian beam waves, Opt. Express 20 (12) (2012) 13055–13064.

[10] X. Liu, S. Chandrasekhar, T.H. Wood, R.W. Tkach, P.J. Winzer, E.C. Burrows, A.R. Chraplyvy, M-ary pulse-position modulation and frequency-shift keying with additional polarization/phase modulation for high-sensitivity optical transmission, Opt. Express 19 (26) (2011) B868–B881.

[11] E. Agrell, M. Karlsson, Power-efficient modulation formats in coherent transmission systems, IEEE/OSA J. Lightwave Technol. 27 (22) (2009) 5115–5126.

[12] M. Karlsson, E. Agrell, Generalized pulse-position modulation for optical power-efficient communication, in: 37th European Conference and Exhibition on Optical Communication (ECOC), Geneva, 2011, pp. 1–3.

[13] X. Liu, T.H. Wood, R.W. Tkach, S. Chandrasekhar, Demonstration of record sensitivity in an optically pre-amplified receiver by combining PDM-QPSK and M-ary pulse-position modulation, IEEE/OSA J. Lightwave Technol. 30 (4) (2012) 406–413.

[14] H. Selmy, H.M.H. Shalaby, Z. Kawasaki., Proposal and performance evaluation of a hybrid BPSK-modified MPPM technique for optical fiber communications systems, IEEE/OSA J. Lightwave Technol. 31 (22) (2013) 3535–3545.

[15] H. Selmy, H.M. Shalaby, Z. Kawasaki, Enhancing optical multipulse pulse position modulation using hybrid QPSK-modified MPPM, in: 2014 IEEE Photonics Conference (IPC), San Diego, CA, USA, 2014, pp. 617–618.

[16] H.S. Khallaf, H.M.H. Shalaby, Z. Kawasaki, Proposal of a hybrid OFDM-PPM technique for free space optical communications systems, in: 2013 IEEE Photonics Conference (IPC), Bellevue, WA, USA, 2013, pp. 287–288.

[17] H.S. Khallaf, H.M.H. Shalaby, Proposal of a hybrid QAM-MPPM technique for optical communications systems, in: Proc. 16th Int. Conf. Transparent Optic. Netw. (ICTON), Graz, Austria, 2014, pp. Tu.B1.7(1–4).

[18] A.E. Morra, H.M.H. Shalaby, S.F. Hegazy, S.S.A. Obayya, Hybrid direct-detection differential phase shift keying-multipulse pulse position modulation techniques for optical communication systems, Opt. Commun. 357 (15) (2015) 86–94.

[19] H.M.H. Shalaby, Maximum achievable constrained power efficiencies of MPPM-LQAM techniques, IEEE Photonics Technol. Lett. 27 (12) (2015) 1265–1268.

[20] A.E. Morra, M. Rihan, A.E. El-Fiqi, H.M.H. Shalaby, S.S.A. Obayya, Evaluation of power efficiency of hybrid modulation techniques, in: 2016 IEEE Photonics Conference (IPC), Bellevue, WA, USA, 2016, pp. 33–34.

[21] E. Nistazakis, A.N. Stassinakis, S.S. Muhammad, G.S. Tombras, BER estimation for multi hop ROFSO QAM or PSK OFDM communication systems over gamma-gamma or exponentially modeled turbulence channels, Opt. Laser Technol. 64 (2014) 106–112.

[22] H.E. Nistazakis, A.N. Stassinakis, H.G. Sandalidis, G.S. Tombras, QAM and PSK OFDM RoFSO Over M-turbulence induced fading channels, IEEE Photonics J. 7 (1) (2015) 1–11.

[23] P. Wang, B. Yang, L. Guo, T. Shang, SER performance analysis of MPPM FSO system with three decision thresholds over exponentiated Weibull fading channels, Opt. Commun. 354 (1) (2015) 1–8.

[24] H.S. Khallaf, H.M.H. Shalaby, J.M. Garrido-Balsells, S. Sampei, Performance analysis of a hybrid QAM-MPPM technique over turbulence-free and Gamma–Gamma free-space optical channels, IEEE/OSA J. Opt. Commun. Networking 7 (2) (2017) 161–171.

[25] K. Cho, D. Yoon, W. Jeong, M. Kavehrad, BER analysis of arbitrary rectangular QAM, in: Conference Record of the 35th Asilomar Conference on Signals, Systems and Computers, Pacific Grove, CA, USA, 2001, pp. 1056–1059.

[26] K. Kiasaleh, On the probability density function of signal intensity in freespace optical communications systems impaired by pointing jitter and turbulence, Opt. Eng. 33 (11) (1994) 3748–3757.

[27] E. Bayaki, D.S. Michalopoulos, R. Schober, EDFA-based all-optical relaying in free-space optical systems, IEEE Trans. Commun. 60 (12) (2012) 3797–3807.

[28] N. Chatzidiamantis, D. Michalopoulos, E. Kriezis, G. Karagiannidis, R. Schober, Relay selection protocols for relay-assisted free-space optical systems, IEEE/OSA J. Opt. Commun. Networking 5 (1) (2013) 92–103.

[29] M. Abaza, R. Mesleh, A. Mansour, E.-H. Aggoune, Performance analysis of MISO multi-hop FSO links over log-normal channels with fog and beam divergence attenuations, Opt. Commun. 334 (1) (2015) 247–252.

[30] A. Bekkali, C.B. Naila, K. Kazaura, K. Wakamori, M. Matsumoto, Transmission analysis of OFDM-based wireless services over turbulent radio-on-FSO links modeled by Gamma-Gamma distribution, IEEE Photonics J. 2 (3) (2010) 510–520.

[31] C. Smorynski, T A Treatise on the Binomial Theorem, first ed., College Publications, 2012.

[32] Wolfram Function Site. (2017, Mar.). [Online]. Available: http://functions.wolfram.com/.

[33] P. Wang, J. Qin, L. Guo, Y. Yang, BER performance of FSO limited by shot and thermal noise over exponentiated Weibull fading channels, IEEE Photonics Technol. Lett. 28 (3) (2016) 252–255.

[34] M. Abramowitz, I.A. Stegun (Eds.), Handbook of Mathematical Functions, tenthe ed., Dover Publications, 1972.

[35] I.M. Gradshteyn, I.S. Ryzhik, Table of Integrals, Series and Products, seventh ed., Academic Press, 2007.

[36] V.S. Adamchik, O.I. Marichev, The algorithm for calculating integrals of hypergeometric type functions and its realization in REDUCE system, in: Proc. of the International Symposium on Symbolic and Algebraic Computation "ISSAC '90", Tokyo, Japan, 1990, pp. 212 –224.